Ilkogretim Online - Elementary Education Online, 2020; Vol 19 (Issue 4): pp. 4755-4764
http://ilkogretim-online.org
doi: 10.17051/ilkonline.2020.04.764881

Majority Voting -Based Detection And Analysis Of Chest X-Ray Images For COVID-19 And Other Infectious Diseases Using Classifiers

Pratibha Sambhakar
M. Tech. Scholar
School of Engineering and I.T., MATS University, Raipur
Apurv Verma
Assistant Professor
School of Engineering and I.T., MATS University, Raipur
Dr. Abhishek Badholia
Associate Professor
School of Engineering and I.T., MATS University, Raipur

Abstract

Most difficult challenge across our planet is novel coronavirus infection (COVID-19). This infection is induced by severe acute respiratory syndrome coronavirus-2 (SARS-COV-2) & has a substantial sickness and death rate over the entire globe. According to the research, contaminated individuals had distinctive radiographic pictorial features as well as temperature, dried coughs, lethargy, breathlessness, and other symptoms. The chest X-ray (CXR) is among the significant, non-intrusive scientific auxiliary which contributes in detecting certain pictorial biological effects correlated with SARS-COV-2 contagion. Moreover, the scarcity of skilled radiologists in interpretation CXR pictures and the inconspicuous presentation of diseases radiographic patterns continue to be the most significant barriers in conventional diagnostic. We describe an automated COVID screenings (ACoS) method that leverages discriminant level of risk collected from CXR photographs to distinguish between ordinary, suspicious, and COVID-19 contaminated individuals in this investigation. The suggested methodology employs a 2 classifying method (natural versus unnatural and COVID-19 versus lung disease) utilising a classifying model group of 5 standard supervised classifying methods centered on majority rule. The ACoS system's training, evaluation, and validation were carried out utilizing 2088. CXR pictures (696 normal, 696 pneumonia, and 696 nCOVID-19) and 258 (86 photos from each group) The validation findings for Stage-I (accuracy (ACC) = 98.062 percent, area under curve (AUC) = 0.956) and Stage-II (ACC = 91.329 percent and AUC = 0.831) suggest that the proposed system performs well. Furthermore, the Friedman post-hoc multiple comparisons and z-test statistics show that the ACoS system findings are statistically significant. Finally, the achieved performance is compared to the state-of-the-art approaches currently in use.

I. Introduction

Covid-19 is a fast transmitting contagious illness which affects not just people and often also pets. Such lethal viral illness has an impact on people's everyday lives, wellness, as well as the economic growth of the world. Covid-19 is a widely prevalent illness. According to a clinical research of COVID-19 infected individuals, these people are generally affected by such acute respiratory infections after getting into touch from this certain virus. Chest x-ray (also known as radiography) & CT Scan seem to be more efficient visualisation technologies for identifying lungs issues. Nonetheless, a significant chest x-ray is a less expensive procedure than a chest CT. Deep learning(DL) is the most effective machine learning approach, providing valuable evaluation to examine a huge number of chest x-ray pictures, who may have a significant influence for Covid-19 monitoring. We used the PA view of x rays scanning for covid-19 sick people and also normal individuals inside this investigation. We evaluated the ability of DL-Based CNN algorithm after clearing out all pictures as

Ilkogretim Online - Elementary Education Online, 2020; Vol 19 (Issue 4): pp. 4755-4764
http://ilkogretim-online.org
doi: 10.17051/ilkonline.2020.04.764881
well as using data augmentation. To assess the effectiveness of the algorithm, 6432 chests x-ray scanning datasets got acquired through the Kaggle database, where this 5467 was utilised for teaching and 965 for validity.
This suggested method is primarily intended for use by a medical professional in the early detection of Covid-19 contaminated individuals. The scientists used a DL algorithm on a chest CT scans datasets to determine the effects of Covid-19 among those who had other lungs illness. Furthermore, in [28], a research presents a research evaluating the effect of covid-19 on kidneys as well as extreme renal dysfunction. In [29], researchers looked at a datasets of 50 individuals whom have Covid-19 illness and were divided into two treatment associations (i.e., good and poor). The dynamics of antigenic and virulent transmission were investigated. The researchers subsequently discovered the health hazard of poor healing as well as pulmonary disease. As a consequence, researchers determined approximately 58% of the individuals seemed to have a weak recuperation. researchers of [30] conducted a research on the overall numbers of people affected with Covid-19 as well as deaths worldwide. investigators [31] proposed a DL-Based algorithm for detecting Covid-19-infected individuals utilizing X-ray pictures. Such approach is useful for medical professionals in recognising symptoms of covid-19 infection in individuals as soon as possible. They discover 97% recognition rate of the developed method for lungs categorization using various matrix dimensions. The researchers in [32] explained where a new corona virus was discovered as an unique respiratory infection in Wuhan, China. The major goal of research was to demonstrate a novel DL system, COVIDX-Net, to assist healthcare practitioners in autonomously diagnosing Covid-19 illness utilizing X-ray pictures.

2. Materials and methods

2.1. Data acquisition, preprocessing, and augmentation

We collected information via 3 open sources inside this research: COVID Chest X-ray set [13], Montgomery set [24], and NIH Chest X-ray14 set [27]. Table 2 shows the full data for the quantity of posterior-anterior (PA) views CXR pictures utilized from all database. All inputs pictures are refined, that contains picture scaling (512 x 512 px), formats conversions (PNG), and colour space conversion (Gray Scale). To decrease the intrinsic quantum noise, the pattern conserving guided filter is used. The de-noising filters was chosen depending on prior research [3].

Table 1: Estimates of its numbers of CXR pictures utilized for efficiency evaluations in the learning, tests, & validating sets across the various repository.

Dataset property	COVID Chest X-ray Set	Montgomery Set	NIH Chest X-ray14 Set	Augmented images	Training -Testing set (80%)	Validation set (20%)
Total Number of X-ray images	542	80	680	1044	2088	258
Number of normal X-ray images	19	80	335	348	696	86
Number of Pneumonia X-ray images	89	–	345	348	696	86
Number of nCOVID-19 CXR images	434	–	–	348	696	86

We separated the pre-processed pictures across 2 subgroups: the learning group (80%) as well as the validating group (20%). Furthermore, the image augmentation methodology is applied towards the pictures in the learning validating group in order to construct a generalized framework by integrating any variance in the pictures that may arise due to different visualization settings. As shown in Table 2, we used several random photometric modifications with spontaneous factors b/w desired bandwidths.

Table 2: Different radiometric adjustments are used to enhance the photograph

Transformations	Range	
Contrast adjustment	Automatic	Adjust the contrast of the image.
Brightness	-20 to 20	Randomly increase or decrease the pixel's intensity between the given range.
Gaussian Blur	0.1 to 1.5	Random smoothing of texture information between the specified range of sigma.
Sharpening	Automatic	Highlight the fine details by adjusting the contrast between bright and dark pixels.

2.2. Acquisition & selecting certain properties

With CXR imaging, COVID-19 affected individuals have uneven surface opacities (Fig. 2 a), respiratory acquisitions (Fig. 2c), reticulonodular opacities (Fig. 2b), and other radiometric textural abnormalities [22]. Radio sensor textural characteristics can be used to express these modest visual qualities. Eight first-order statistical features (FOSF), 88 grey level co-occurrence matrix (GLCM) ([17], [19]) features (in four different orientations), and 8100 histograms of oriented gradients (HOG) ([15]) features are used in this investigation. The FOSF uses the mean, variance, roughness, smoothness, kurtosis, energy, and entropy, among other things, to describe the entire images at a look. It can measure worldwide textural structures, but it doesn't take into account local neighborhoods data. The GLCM and HOG feature descriptors are utilised to do in-depth texture analysis to solve this issue. The GLCM feature describes the spatial correlation between pixel intensities in radiographic texture patterns in four different directions (i.e. 0°, 45°, 90°, 135°), whereas the HOG feature stores local shape/texture information. These statistical texture features were chosen because they can encode natural texture patterns and are commonly employed in medical picture analysis ([4], [5]).

Ilkogretim Online - Elementary Education Online, 2020; Vol 19 (Issue 4): pp. 4755-4764
http://ilkogretim-online.org
doi: 10.17051/ilkonline.2020.04.764881

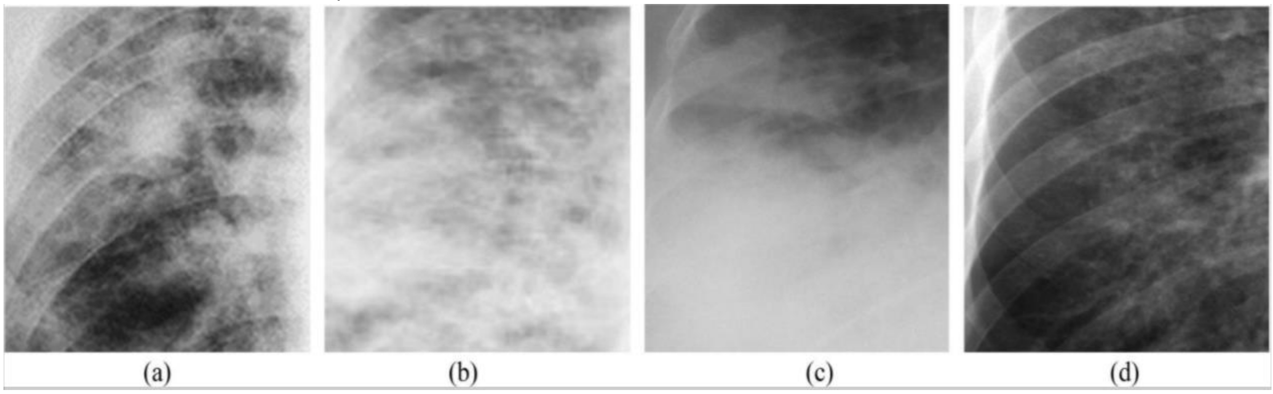

Figure 1: Pictures of COVID-19-infected chest X-rays

(a) Ground-glass ambiguity, (b) Reticular ambiguity, (c) Cardiovascular consolidation, (d) Mild ambiguity

2.5. Metrics for evaluating effectiveness

The suggested ACoS system's effectiveness would be evaluated employing seven performance standards, as per Eq 9-15 [18], in which true positive (TP) and true negative (TN) represents the amount of contaminated and totally natural CXR pictures accurately forecasted by proposed model, respectively; false positive (FP) and false-negative (FN) signify the misdiagnosis of natural as well as contaminated visuals, in consequence;

P = TP + FN and N = TN + FP.

$$\text{Accuracy(ACC)} = \frac{\text{TP} + \text{TN}}{\text{P} + \text{N}} \times 100 \quad 9$$

$$\text{Specificity} = \frac{\text{TN}}{\text{N}} \times 100 \quad 10$$

$$\text{Precision} = \frac{\text{TP}}{\text{TP} + \text{FP}} \times 100 \quad 11$$

$$\text{Recall} = \frac{\text{TP}}{\text{P}} \times 100 \quad 12$$

$$\text{F1} - \text{Measure} = \frac{2 \times \text{precision} \times \text{recall}}{\text{precision} + \text{recall}} \times 100 \quad 13$$

$$\text{AreaUnderCurve(AUC)} = \left(\frac{\text{TP}}{\text{P}} + \frac{\text{TN}}{\text{N}}\right) \quad 14$$

Ilkogretim Online - Elementary Education Online, 2020; Vol 19 (Issue 4): pp. 4755-4764
http://ilkogretim-online.org
doi: 10.17051/ilkonline.2020.04.764881

$$\text{MatthewsCorrelationCoefficient(MCC)} = \frac{\mathrm{TP} \times \mathrm{TN} - \mathrm{FP} \times \mathrm{FN}}{\sqrt{(\mathrm{TP} + \mathrm{FP}) \times \mathrm{P} \times \mathrm{N} \times (\mathrm{TN} + \mathrm{FN})}} \qquad 15$$

Moreover, the acquired findings are statically confirmed by applying z-test and Friedman average ranking, as well as the posthoc various comparisons methodologies of Holm (Holm, 1979) and Shaffer (Shaffer, 1986).

3. Evaluation of the outcomes of the experiments

This section contains a detailed summary of the testing results for the recommended ACoS systems. The investigations that follow are intended to put the hypothetical assumptions to the assessment (Theory 1, Theory 2, and Theory 3):

To distinguish the natural, COVID-19, & other respiratory infections X-ray pictures in this investigation, we employed a two-stage categorization methodology. Applying raw CXR pictures from training-testing set, two pairs of classification algorithm are generated for stage I & stage II, sequentially. Following that, picture enhancement being carried out utilizing various optical adjustments as described in Part 2.1. Those enhanced pictures are combined with raw CXR pictures to re-educate training algorithms then analyze recognition accuracy. According to the results in Tables 4 and 5, the supervised algorithms conditioned with enhanced pictures functioned much superior than the algorithms trainned with raw CXR pictures for both stages (stage I & II), confirming the correctness of Theory 1. The encouraging results observed with enhanced pictures may be explained from such facts that enhanced photos give enough examples to educate the models for probable variances in inputs CXR pictures that may arise owing to varied screening settings and equipment at various health centers.

Table 3: The test dataset was used to test the effectiveness of several supervised algorithms as well as the majority voter's technique in Stage I (Normal vs. Abnormal) classifications.

Classification algorithms	Accuracy (%)	Specificity (%)	Precision (%)	Recall (%)	F_1-Measure (%)	AUC	MCC
Majority voting	98.062	96.512	98.266	98.837	98.551	0.977	0.956
ANN	96.512	93.023	96.571	98.256	97.406	0.956	0.921
SVM (Poly Kernel)	96.124	91.860	96.023	98.256	97.126	0.951	0.912
SVM (Linear Kernel)	96.124	90.698	95.506	98.837	97.143	0.948	0.913
KNN	95.736	94.186	97.076	96.512	96.793	0.953	0.904
SVM (RBF Kernel)	95.349	89.535	94.944	98.256	96.571	0.939	0.895
DT	90.698	80.233	90.659	95.930	93.220	0.881	0.788

NB	88.372	73.256	87.766	95.930	91.667	0.846	0.734

In Stage II, all supervised algorithm was used to classify the aberrant inputs pictures, and such predictions outcomes are combined with a majority voting-based classifiers combination. In comparison to standalone algorithms, the majority voting classifiers combination showed much greater efficiency (ACC of 91.279 percent, AUC of 0.913, and MCC of 0.830) since presented on Table 4. This shows the efficiency of the suggested ACoS method (demonstrating the truthfulness of Theory 3).

Table 4: The validating dataset was used to test the performances of multiple supervised classifiers as well as the majority voting methodology in stage-II (COVID ” versus “ Respiratory infections) classifications.

Classification algorithms	**Accuracy (%)**	**Recall (%)**	**Precision (%)**	**F_1-Measure (%)**	**Specificity (%)**	**AUC**	**MCC**
Majority voting	**91.329**	**96.512**	**87.368**	**91.713**	**86.207**	**0.914**	**0.831**
SVM (RBF Kernel)	86.628	89.535	84.615	87.006	83.721	0.866	0.734
SVM (Poly Kernel)	86.047	93.023	81.633	86.957	79.070	0.860	0.728
SVM (Linear Kernel)	81.977	80.233	83.133	81.657	83.721	0.820	0.640
NB	80.814	89.535	76.238	82.353	72.093	0.808	0.626
DT	79.070	75.581	81.250	78.313	82.558	0.791	0.583
ANN	73.256	93.023	66.667	77.670	53.488	0.733	0.506
KNN	72.093	67.442	74.359	70.732	76.744	0.721	0.444

To take a detour from the nCOVID-19's communities spreading, one among the desirable qualities in any ACoS systems and it has the fewest Type-II (false negative) mistakes while maintaining the highest amount of Type-I (false positive) mistakes. Employing a test set, Fig. 4 (a) and (b) illustrate the confusion matrix (CM) for the majority voting method for Stage-I and Stage-II, correspondingly. This majority vote technique outperforms all those, resulting in less Type-I and Type-II mistakes, according to the CM.

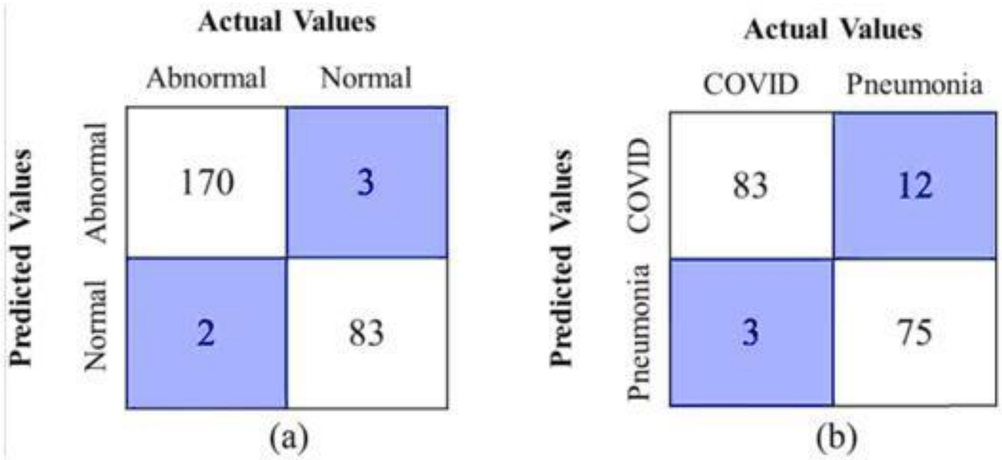

Figure 2: Applying a training dataset to create a confusion matrix (a) Stage-I, (b) Stage-II.

3.2. Explanation

Millions of deaths have been documented globally as a result of COVID-19-related incidence and fatality. This contagion is already being designated a worldwide medical disaster by the WHO (Coronavirus Disease 2019, 2020). We introduced an ACoS system that uses CXR images information to track COVID-19 afflicted individuals inside this research. To separate healthy, COVID-19, and pneumonia infection pictures, we used a two-stage classification algorithm. The following were the primary problems we faced during our research:

- The COVID-19 contaminated CXR pictures that are publically accessible are restricted and poor uniformity.
- COVID-19 and respiratory diseases have unclear radiographic features.
- Prior analyzing, reconfigure all incoming CXR pictures to a smaller length and width (such as 64x64 or 224x224, and so on.) to avoid losing critical prejudicial textural features
- To adequately build the machine, it need a large amount of learning knowledge
- Experience is required to create appropriate networks design and configure the numerous hyper-parameters (like input resolution, number of layers, filters, and filter shape, etc.).
- It takes a significant amount of computational capacity, a fair amount of storage, as well as a huge amount of time for training that system.
- Apart from traditional machine learning, DL techniques were hard to describe.

4. Conclusion

We had proposed an ACoS approach for the diagnostic test for COVID-19 infectious diseases inside this research, as then appropriate preventative actions (such as social exclusion and RT-PCR testing) may be done to avoid the disease from spreading moreover. This research outcomes were summarised:

- The proposed ACoS system showed promise in segregating normal, respiratory disease, and COVID-19-infected sick people, as evidenced by the significant performance of Stage-I (ACC = 98.062 percent, AUC = 0.977, and MCC = 0.956) and Stage-II (ACC = 91.329 percent, AUC = 0.914, and MCC = 0.831) utilising training dataset.
- Due to varying imaging settings in different hospitals, there are considerable differences in the input CXR pictures. The suggested approach made advantage of enhanced pictures, which provided enough diversity to train and increase the model's resilience.

- FOSF, GLCM, and HOG properties were radiomic textural identifiers that are very effective in quantifying the connection properties of radiometric optical properties linked to COVID-19 infections.
- Apart from data-hungry deep learning techniques, the suggested ACoS system employed traditional machine learning methods to develop the classifier using less labeled photos & computer assets. Such sort of technology will be much more clinically acceptable and could be implemented also within an resource restrained surroundings.
- Friedman posthoc multi comparisons and z-score statics corroborate the suggested program statistically significant.

The report's further development must aim to increase the program's dependability as well as medical acceptance. The CAD system's combination of the individual patient symptoms as well as the radiologist's comments might aid in the development of a viable screening programme In addition, a detailed analytical comparative analysis across traditional techniques and deep learning approaches might aid in determining medical acceptance.

References

[1] Abbas, A., Abdelsamea, M. M., & Gaber, M. M. (2020). Classification of COVID-19 in chest X-ray images using DeTraC deep convolutional neural network. Retrieved from http://arxiv.org/abs/2003.13815.

[2] Altaf F., Islam S.M.S., Akhtar N., Janjua N.K. Going deep in medical image analysis: Concepts, methods, challenges and future directions. IEEE Access. 2019;7:99540–99572. http://arxiv.org/abs/1902.05655 Retrieved from. [Google Scholar]

[3] Chandra T.B., Verma K. Pneumonia Detection on Chest X-Ray Using Machine Learning Paradigm. In: Chaudhuri B.B., Nakagawa M., Khanna P., Kumar S., editors. Proceedings of third international conference on computer vision & image processing. Springer; Singapore: 2020. pp. 21–33. [CrossRef] [Google Scholar]

[4] Chandra T.B., Verma K., Jain D., Netam S.S. 2020 First international conference on power, control and computing technologies (ICPC2T) IEEE; 2020. Localization of the suspected abnormal region in chest radiograph images; pp. 204–209. [CrossRef] [Google Scholar]

[5] Chandra T.B., Verma K., Singh B.K., Jain D., Netam S.S. Automatic detection of tuberculosis related abnormalities in Chest X-ray images using hierarchical feature extraction scheme. Expert Systems with Applications. 2020;158 doi: 10.1016/j.eswa.2020.113514. [CrossRef] [Google Scholar]

[6] Chatterjee S., Dey D., Munshi S. Integration of morphological preprocessing and fractal based feature extraction with recursive feature elimination for skin lesion types classification. Computer Methods and Programs in Biomedicine. 2019;178:201–218. doi: 10.1016/j.cmpb.2019.06.018. [PubMed] [CrossRef] [Google Scholar]

[7] Chen Q., Meng Z., Su R. WERFE: A gene selection algorithm based on recursive feature elimination and ensemble strategy. Frontiers in Bioengineering and Biotechnology. 2020;8:496. doi: 10.3389/fbioe.2020.00496. [PMC free article] [PubMed] [CrossRef] [Google Scholar]

[8] Chen N., Zhou M., Dong X., Qu J., Gong F., Han Y.…Zhang L. Epidemiological and clinical characteristics of 99 cases of 2019 novel coronavirus pneumonia in Wuhan, China: A descriptive study. The Lancet. 2020;395(10223):507–513. doi: 10.1016/S0140-6736(20)30211-7. [PMC free article] [PubMed] [CrossRef] [Google Scholar]

[9] Cheng S.-C., Chang Y.-C., Fan Chiang Y.-L., Chien Y.-C., Cheng M., Yang C.-H.…Hsu Y.-N. First case of Coronavirus Disease 2019 (COVID-19) pneumonia in Taiwan. Journal of the Formosan Medical Association. 2020;119(3):747–751. doi: 10.1016/j.jfma.2020.02.007. [PMC free article] [PubMed] [CrossRef] [Google Scholar]

[10] Chouhan V., Singh S.K., Khamparia A., Gupta D., Tiwari P., Moreira C.…de Albuquerque V.H.C. A novel transfer learning based approach for pneumonia detection in chest X-ray images. Applied Sciences (Switzerland) 2020;10(2) doi: 10.3390/app10020559. [CrossRef] [Google Scholar]

[11] Chowdhury, M. E. H., Rahman, T., Khandakar, A., Mazhar, R., Kadir, M. A., Mahbub, Z. Bin, … Reaz, M. B. I. (2020). Can AI help in screening Viral and COVID-19 pneumonia? (March). Retrieved from http://arxiv.org/abs/2003.13145.

[12] Chung M., Bernheim A., Mei X., Zhang N., Huang M., Zeng X.…Shan H. CT imaging features of 2019 Novel Coronavirus (2019-nCoV) Radiology. 2020;295(1):202–207. doi: 10.1148/radiol.2020200230. [PMC free article] [PubMed] [CrossRef] [Google Scholar]

[13] Cohen, J. P., Morrison, P., & Dao, L. (2020). COVID-Chestxray Database. Retrieved June 20, 2020, from https://github.com/ieee8023/covid-chestxray-dataset.

[14] Coronavirus Disease 2019. (2020). Retrieved April 8, 2020, from World Health Organization website: https://www.who.int/emergencies/diseases/novel-coronavirus-2019.

[15] Dalal N., Triggs B. In 2005 IEEE computer society conference on computer vision and pattern recognition (CVPR'05) Vol. 1. 2005. Histograms of oriented gradients for human detection; pp. 886–893. [CrossRef] [Google Scholar]

[16] Emary E., Zawbaa H.M., Hassanien A.E. Binary grey wolf optimization approaches for feature selection. Neurocomputing. 2016;172:371–381. doi: 10.1016/j.neucom.2015.06.083. [CrossRef] [Google Scholar]

[17] Gómez W., Pereira W.C.A., Infantosi A.F.C. Analysis of co-occurrence texture statistics as a function of gray-level quantization for classifying breast ultrasound. IEEE Transactions on Medical Imaging. 2012;31(10):1889–1899. doi: 10.1109/TMI.2012.2206398. [PubMed] [CrossRef] [Google Scholar]

[18] Han J., Kamber M., Pei J. Data mining: Concepts and techniques. Morgan Kaufmann; San Francisco, CA, itd: 2012. [CrossRef] [Google Scholar]

[19] Haralick R.M., Shanmugam K., Dinstein I. Textural features for image classification. IEEE Transactions on Systems, Man, and Cybernetics. 1973;SMC-3(6):610–621. doi: 10.1109/TSMC.1973.4309314. [CrossRef] [Google Scholar]

[20] Ho T.K., Gwak J. Multiple feature integration for classification of thoracic disease in chest radiography. Applied Sciences. 2019;9(19):4130. doi: 10.3390/app9194130. [CrossRef] [Google Scholar]

[21] Holm S. A simple sequentially rejective multiple test procedure. Scandinavian Journal of Statistics. 1979;6:65–70. [Google Scholar]

[22] Hosseiny M., Kooraki S., Gholamrezanezhad A., Reddy S., Myers L. Radiology perspective of coronavirus disease 2019 (COVID-19): Lessons from severe acute respiratory syndrome and middle east

respiratory syndrome. American Journal of Roentgenology. 2020;(October):1–5. doi: 10.2214/AJR.20.22969. [PubMed] [CrossRef] [Google Scholar]

[23] Huang C., Wang Y., Li X., Ren L., Zhao J., Hu Y.…Cao B. Clinical features of patients infected with 2019 novel coronavirus in Wuhan, China. The Lancet. 2020;395(10223):497–506. doi: 10.1016/S0140-6736(20)30183-5. [PMC free article] [PubMed] [CrossRef] [Google Scholar]

[24] Jaeger S., Karargyris A., Candemir S., Folio L., Siegelman J., Callaghan F.…McDonald C.J. Automatic tuberculosis screening using chest radiographs. IEEE Transactions on Medical Imaging. 2014;33(2):233–245. doi: 10.1109/TMI.2013.2284099. [PubMed] [CrossRef] [Google Scholar]

[25] Jaiswal A.K., Tiwari P., Kumar S., Gupta D., Khanna A., Rodrigues J.J.P.C. Identifying pneumonia in chest X-rays: A deep learning approach. Measurement: Journal of the International Measurement Confederation. 2019;145:511–518. doi: 10.1016/j.measurement.2019.05.076. [CrossRef] [Google Scholar]

[26] Hemdan, E. E.-D., Shouman, M. A., & Karar, M. E. (2020). COVIDX-Net: A framework of deep learning classifiers to diagnose COVID-19 in X-Ray images. Retrieved from http://arxiv.org/abs/2003.11055.

[27] Kanne J.P., Little B.P., Chung J.H., Elicker B.M., Ketai L.H. Essentials for radiologists on COVID-19: An update-radiology scientific expert panel. Radiology. 2020;200527 doi: 10.1148/radiol.2020200527. [PMC free article] [PubMed] [CrossRef] [Google Scholar]

[28] Ke Q., Zhang J., Wei W., Połap D., Woźniak M., Kośmider L., Damaševĭcius R. A neuro-heuristic approach for recognition of lung diseases from X-ray images. Expert Systems with Applications. 2019;126:218–232. doi: 10.1016/j.eswa.2019.01.060. [CrossRef] [Google Scholar]

[29] Khatami A., Khosravi A., Nguyen T., Lim C.P., Nahavandi S. Medical image analysis using wavelet transform and deep belief networks. Expert Systems with Applications. 2017;86:190–198. doi: 10.1016/j.eswa.2017.05.073. [CrossRef] [Google Scholar]

[30] Shukla, A., Kalnoor, G., Kumar, A., Yuvaraj, N., Manikandan, R., & Ramkumar, M. (2021). Improved recognition rate of different material category using convolutional neural networks. Materials Today: Proceedings. Published. https://doi.org/10.1016/j.matpr.2021.04.307

[31] Mishra, A., Jain, H., Biswas, P., Thowseaf, S., & Manikandan, R. (2021). Integrated solution for optimal generation operation efficiency through dynamic economic dispatch on Software Technological Park of India. Materials Today: Proceedings. Published. https://doi.org/10.1016/j.matpr.2021.05.019